nature neuroscience

SeeDB: a simple and morphology-preserving optical clearing agent for neuronal circuit reconstruction

Meng-Tsen Ke[1,2], Satoshi Fujimoto[1] & Takeshi Imai[1–3]

We report a water-based optical clearing agent, SeeDB, which clears fixed brain samples in a few days without quenching many types of fluorescent dyes, including fluorescent proteins and lipophilic neuronal tracers. Our method maintained a constant sample volume during the clearing procedure, an important factor for keeping cellular morphology intact, and facilitated the quantitative reconstruction of neuronal circuits. Combined with two-photon microscopy and an optimized objective lens, we were able to image the mouse brain from the dorsal to the ventral side. We used SeeDB to describe the near-complete wiring diagram of sister mitral cells associated with a common glomerulus in the mouse olfactory bulb. We found the diversity of dendrite wiring patterns among sister mitral cells, and our results provide an anatomical basis for non-redundant odor coding by these neurons. Our simple and efficient method is useful for imaging intact morphological architecture at large scales in both the adult and developing brains.

Although fluorescent proteins can be used to genetically label cellular and subcellular architecture *in vivo*, sample opacity often limits imaging deep inside the tissue. This is particularly problematic when biological samples are fixed with paraformaldehyde. Even with two-photon microscopy, fixed brain samples can be imaged up to only a depth of approximately 300 μm (ref. 1). Sample opacity is caused by both light absorption and scattering, but the latter is the larger problem when imaging mammalian tissues.

To reduce the amount of light scattering in tissues, several optical clearing agents have been developed. Scattering occurs when the refractive index of scatter differs from the medium[2]. The refractive indices of scatter in fixed tissues are much higher (~1.5) than water (1.33)[3]. Thus, high-index solvents, such as BABB (Murray's clear, a 1:2 mixture of benzyl alcohol and benzyl benzoate, refractive index = 1.56), methyl salicylate (1.52), dibenzyl ether (1.56), 2,2′-thiodiethanol (1.52) and glycerol (1.47) have been used for optical clearing after whole-mount antibody staining[4–9]. However, these optical clearing agents quench fluorescent proteins because these proteins require water molecules to fluoresce. Another approach for optical clearing is tissue maceration, in which potassium hydroxide or trypsin is used for partial protein digestion and denaturation to facilitate optical clearing[10,11]. Recently, an optical clearing agent was reported, Sca*l*e, which contains urea[12]. Because fluorescent proteins are stable in the urea solution, the Sca*l*e method was able to image fluorescent proteins deep inside the tissues of fixed mouse brains. This method, however, requires a long incubation time for clearing, from weeks to months. In addition, a large expansion in sample volume compromises the detailed cellular morphology as well as the real depth (the depth in the original samples) in many situations in which the working distance of an objective lens is a limiting factor. Furthermore, because urea causes partial denaturation and loss of cellular proteins, the Sca*l*e-treated samples are very fragile and difficult to handle. Thus, a more moderate optical clearing agent is desirable for studying cellular morphology both in fine detail and at large scales with minimal artifacts.

We developed a water-based optical clearing agent, SeeDB (See Deep Brain), which overcomes the limitations seen with other agents, including long incubation times and tissue deformation. Combined with two-photon microscopy, SeeDB allowed us to image fixed mouse brains at the millimeter-scale level. We also used SeeDB to examine the detailed wiring diagram of mitral cells associated with a common glomerulus in the olfactory bulb. The compatibility of SeeDB with fluorescent proteins and various neuronal tracers in fixed tissues should facilitate comprehensive and quantitative analyses for understanding neuronal circuitry.

RESULTS

SeeDB, an optical clearing agent using fructose and thiol

To develop a better optical clearing agent for imaging fluorescent proteins, we sought to use aqueous solutions with refractive indices close to that of fixed tissues[13]. Previously, high-concentration sucrose solutions have been used to reduce light scattering of the brain and invertebrate samples[1,14]. Among the various sugar solutions tested, we found a fructose solution to be an ideal clearing agent. Fructose is highly soluble in water, and the refractive index of a saturated fructose solution reaches 1.490 at 25 °C (80.2% wt/wt, ~115% wt/vol) and 1.502 at 37 °C (86.7% wt/wt, ~130% wt/vol), which are higher than other water-based clearing reagents (**Supplementary Table 1**)[1,6]. As a result, fructose solutions proved to be more effective at clearing tissues than the other clearing agents. Furthermore, we found that high-concentration fructose solutions did not cause the shrinkage of samples that was observed with sucrose solutions[1]. Although longer incubation periods in the fructose solution (>7 d), especially at higher temperatures (for example, 37 °C), caused browning and autofluorescence accumulation as a result of the Maillard reaction[15], these effects could be avoided by adding thiols such as β-mercaptoethanol

[1]Laboratory for Sensory Circuit Formation, RIKEN Center for Developmental Biology, Kobe, Japan. [2]Graduate School of Biostudies, Kyoto University, Kyoto, Japan. [3]PRESTO, Japan Science and Technology Agency, Saitama, Japan. Correspondence should be addressed to T.I. (imai@cdb.riken.jp).

Received 9 April; accepted 27 May; published online 23 June 2013; doi:10.1038/nn.3447

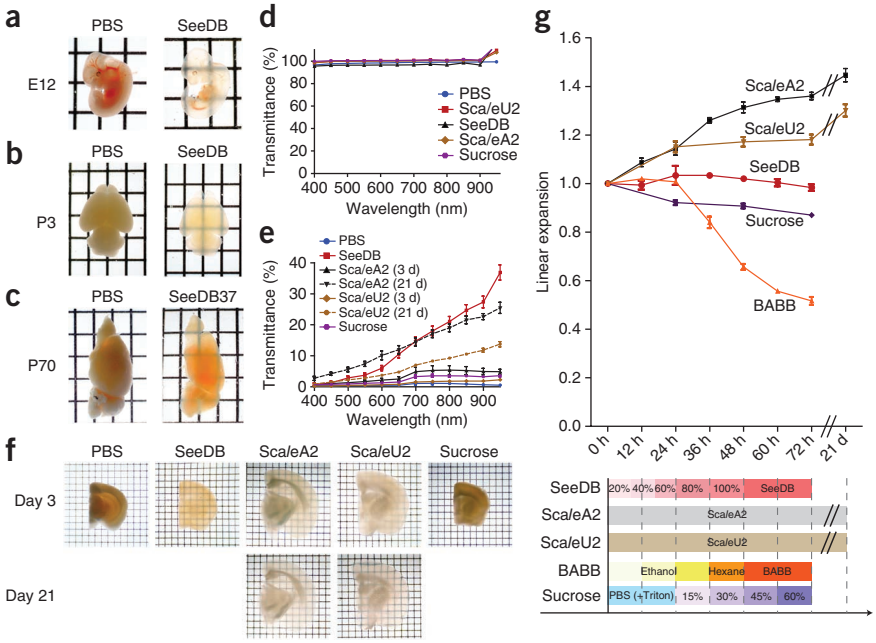

Figure 1 Optical clearing using SeeDB. (**a**) Whole embryos (E12) were cleared with SeeDB using a 3-d clearing protocol (**g**, bottom). (**b**) Neonatal (P3) whole-brain samples cleared with SeeDB (using an optimized protocol for neonatal brain, SeeDBp; **Supplementary Fig. 4**). SeeDB-treated samples kept their original morphology, whereas those treated with Sca*l*eA2 often fell apart during incubation because Sca*l*eA2 causes tissue sample fragility (data not shown). (**c**) Adult hemi-brain samples (P70) cleared with SeeDB37. The images presented in **a**–**c** are transmission images. (**d**) Transmittance curves of various clearing agents (mean ± s.e.m., $n = 3$ measurements). (**e**) Transmittance curves of mouse brain samples cleared with various clearing agents. Myelinated structures in adult brain cause non-homogeneous scattering; we used P21 mouse hemi-forebrain samples because they showed more homogeneous scattering. Transmittance was measured along the medial-lateral axis (the thickest part), which was 5.13 ± 0.19 mm (mean ± s.d., $n = 3$ hemi-forebrains) before clearing. Data are presented as the mean ± s.e.m. ($n = 3$ hemi-forebrains each). (**f**) Adult brain slices (P66, 1.5 mm thick) cleared with various clearing agents (transmission images). Note that white matter was fully cleared with SeeDB, but not with Sca*l*eA2 or Sca*l*eU2. (**g**) Sample expansion and shrinkage during the optical clearing. Hemi-forebrain samples (P21) were cleared with SeeDB, Sca*l*eA2, Sca*l*eU2, sucrose or BABB according to the timeline shown at the bottom. Optical clearing using Sca*l*eA2 caused ~150% sample expansion per dimension. BABB caused ~50% linear sample shrinkage. In contrast, optical clearing with SeeDB did not cause obvious changes in sample volumes. Error bars indicate s.e.m. ($n = 3$ hemi-forebrains each). Grids are 2.6 × 3.2 mm (**a**–**c**) and 1 × 1 mm (**f**).

or α-thioglycerol to the solution (**Supplementary Fig. 1**). Together, these findings led us to establish the clearing agent SeeDB, which is a saturated solution of fructose (80.2% wt/wt) in water with 0.5% α-thioglycerol.

We treated paraformaldehyde-fixed embryo and brain samples with increasing concentrations of aqueous fructose solutions and finally equilibrated them in SeeDB (**Fig. 1**). The entire procedure took approximately 3 d, whereas clearing with Sca*l*eA2 took approximately 3 weeks to clear the mouse brain (**Fig. 1** and **Supplementary Figs. 2** and **3**)[12]. To evaluate tissue transparency, we quantified light transmittance in postnatal day 21 (P21) mouse hemi-forebrain samples, which are less myelinated than adult brains. Brain samples treated with SeeDB were more transparent than those treated with 60% sucrose or Sca*l*eA2 for 3 d and were comparable to those treated with Sca*l*eA2 for 21 d under the light-wavelength range of 400–950 nm (**Fig. 1e**). In adult brain slices, Sca*l*eA2 could not fully clear the white matter of the brain because the lipid-rich myelin structures of white matter have a higher refractive index, whereas SeeDB was able to effectively clear both gray and white matter because its refractive index is close to that of lipids (**Fig. 1f**). Optical clarity of samples was further improved with an 86.7% (wt/wt) fructose solution (SeeDB37), although this solution had to be kept at 37 °C to prevent precipitation of fructose crystals. Although the Sca*l*eA2-treated samples were fragile and often fell apart during incubation (especially embryos and neonatal brains), the SeeDB-treated samples did not show marked fragility (**Fig. 1a**,**b**).

Fine morphological architecture is preserved with SeeDB

Previously reported optical clearing agents also caused large changes to the sample volume. For example, optical clearing by BABB resulted in sample shrinkage during the dehydration process (approximately 50% linear shrinkage for P21 mouse brain), whereas optical clearing by Sca*l*eA2 caused a 150% linear expansion in sample size. Although sample expansion could be reduced using Sca*l*eU2, it required longer incubation times for clearing than with Sca*l*eA2 (**Fig. 1f** and **Supplementary Figs. 2** and **3**)[12]. In contrast, SeeDB did not markedly change sample volumes, remaining relatively constant during and after optical clearing (**Fig. 1g**). To evaluate the changes to morphology resulting from optical clearing, we sparsely labeled a population of mitral cells in the olfactory bulb using fluorescent dextran tracers. After optical clearing with Sca*l*eA2, the dendrites of labeled mitral cells appeared highly serrated, most likely as a result of the anisotropic increase in sample volume (**Fig. 2a**). In contrast, such morphological deformations were not observed in SeeDB-treated samples; the morphology of dendrites remained indistinguishable from those *in vivo* (**Fig. 2a**). Quantitative measurements of dendrite tortuosity also supported this notion (**Fig. 2b**). In the cerebral cortex, even the fine dendritic morphology of pyramidal neurons, including dendritic spines, remained intact after the SeeDB treatment (**Fig. 2c**).

When neonatal brain samples were cleared with the above protocol, we initially observed moderate sample expansion after SeeDB treatment (up to 125% linear expansion, data not shown). We worked to optimize the clearing conditions for the samples and found that adding 0.1× phosphate-buffered saline (PBS) in the 20–80% fructose gradients resulted in minimal changes in sample volume without compromising optical clarity (SeeDBp; **Supplementary Fig. 4**). After establishing optimal conditions, we also tested optical clearing in agarose-embedded samples. Agarose embedding was useful not only to maintain morphology of the fragile samples, but also to mount samples for imaging with an upright microscope (Online Methods and **Supplementary Fig. 5**).

Unlike previous clearing agents, SeeDB does not change the chemical nature of the samples. For example, a comparison of various clearing agents using *Thy1-YFP* line G transgenic mice revealed that fluorescence of cytosolic EYFP was best preserved using SeeDB

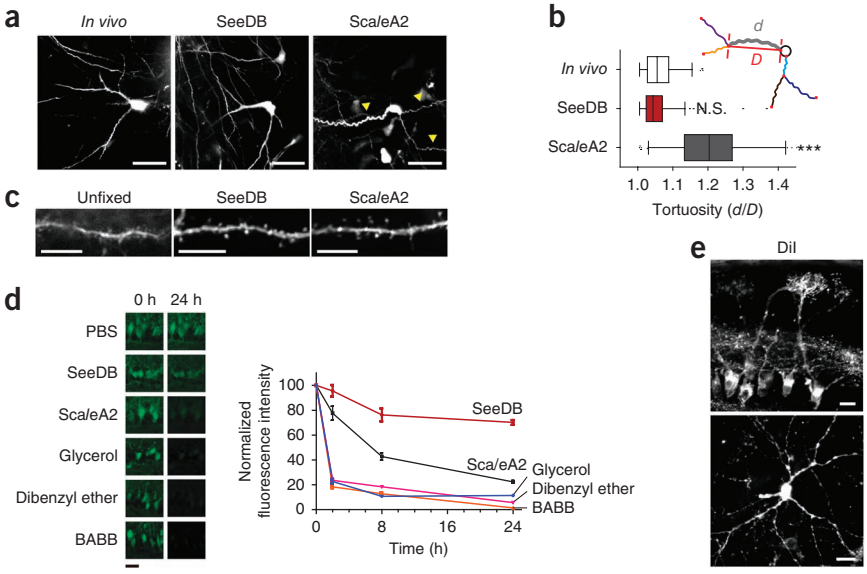

Figure 2 Morphological and chemical stability. (**a**) Morphological changes after optical clearing. Small numbers of mitral cells in the olfactory bulb were labeled with dextran tracers (dextran Alexa 488 for *in vivo* imaging, dextran Alexa 647 for imaging after fixation, 10 kDa). *In vivo* images of the olfactory bulbs in anesthetized mice were acquired using a two-photon microscope with a 25× objective lens (Olympus, XLPLN25XWMP). After optical clearing using SeeDB (3 d) or Sca*l*eA2 (21 d), the olfactory bulbs were imaged using a confocal microscope with a 20× objective lens (Olympus, UPLSAPO20X). Somata and lateral dendrites of mitral cells were imaged. Although lateral dendrites *in vivo* and in SeeDB-treated samples had a smooth appearance, those in Sca*l*eA2-treated samples appeared serrated (yellow arrowheads), suggesting morphological damage as a result of anisotropic sample volume changes. Scale bars, 50 μm. (**b**) Quantification of dendrite deformation shown in **a**. First, we segmented lateral dendrites of mitral cells at perisomatic site, branch point, end point, and end of the image field (red dots in schema). For each dendrite segment, the minimal distance between two ends (*D*) and length of actual trajectory (*d*) were determined. The ratio (*d*/*D*) was calculated as a tortuosity index. Box plots represent lower quartile, median and upper quartile. Bars indicate 5th and 95th percentiles. Data are based on 93–167 dendrite segments from 35–46 neurons in 2 or 3 mice per group. N.S., non-significant ($P > 0.05$); ***$P < 0.001$, compared with *in vivo* (one-tailed Mann-Whitney's *U* test). (**c**) Two-photon images of dendritic spines imaged before and after optical clearing (*Thy1-YFP-H* mice, basal dendrites of layer V pyramidal neurons). A 25× objective lens (Olympus, XLPLN25XSVMP, NA = 1.0) was used. Scale bars, 10 μm. (**d**) Fluorescence of EYFP before and after clearing with various agents (*Thy1-YFP-G* mouse, sections of olfactory bulb). Because quenching kinetics of fluorescent proteins in tissues were different from that of purified fluorescent proteins or in HEK293T cells (data not shown), we used tissue sections of transgenic mice to evaluate the stability of fluorescent proteins. Scale bar, 20 μm. Quantifications of fluorescence intensity for EYFP are shown on the right. Data are presented as mean ± s.e.m. for five regions of interest. A representative result of three independent experiments is shown. Data for other fluorescent proteins are shown in **Supplementary Figure 6**. (**e**) Confocal stacked images of DiI-labeled mitral cells in the olfactory bulb (P5). Primary (top, 95 μm *z* stack) and lateral (bottom, 30 μm *z* stack) dendrites are shown. Whole-mount samples were used for imaging. A 20× objective lens (Olympus, UPLSAPO20X) was used. Scale bars, 20 μm.

(**Fig. 2d** and **Supplementary Fig. 6**). Optical clearing with SeeDB was reversible and could also be combined with immunohistochemistry without loss of antigenicity (**Supplementary Fig. 7**). Furthermore, SeeDB was able to clear brain samples labeled with lipophilic dyes such as DiI, a powerful and commonly used neuronal tracer, because the plasma membrane remains intact (**Fig. 2e** and **Supplementary Fig. 8**); this is an important advantage, as lipophilic dyes are the only choices available for fluorescent neuronal tracing of post-fixed brains.

See Deep Brain: fluorescence imaging of the mouse brains

We next evaluated the imaging depths possible using adult mouse brain samples. We compared optical clarity and fluorescence intensity of SeeDB-treated (for 3 d) and Sca*l*eA2-treated (for 21 d) brain samples using confocal microscopy. We used the adult (P70) *Thy1-YFP* line H mouse[16], and cleared one hemisphere of the brain with SeeDB and the other with Sca*l*eA2. Samples were imaged using a 10× air objective lens (numerical aperture (NA) = 0.4, working distance = 3.1 mm). We obtained images in both samples from the surface of the cerebral cortex to the dentate gyrus of the hippocampus (depth of ~2.3 mm in real samples; **Fig. 3a** and **Supplementary Video 1**).

We then imaged the cleared adult mouse brain samples using two-photon microscopy, which is less sensitive to light scattering than confocal microscopy[2]. Using a commercially available long–working distance objective lens for two-photon microscopy, we were able to image up to depths of approximately 4 mm (limited by working distance) from the dorsal surface of the brain (**Supplementary Fig. 9**). However, because commercially available objective lenses are designed for the refractive index of water or Sca*l*eA2, the image resolution and brightness were reduced in deep regions in SeeDB as a result of spherical aberrations (**Fig. 3f**). Thus, spherical aberration is a major problem to image cleared samples deep inside. To acquire deeper images at higher resolution, we asked a manufacturer to design a long–working distance objective lens (NA = 0.9, working distance = 8 mm) that performs best with the high refractive index of SeeDB. Point-spread function analysis of fluorescent microspheres demonstrated that resolutions decreased in the deep regions in SeeDB when we used objective lenses designed for water or Sca*l*eA2 immersion; in contrast, the resolution remained relatively constant when we used our customized objective lens designed for SeeDB (**Fig. 3g**). Using this customized objective lens, we were able to image SeeDB37-treated adult hemi-brain samples from the dorsal surface of the cerebral cortex to the bottom of the brain (**Fig. 3c–e** and **Supplementary Videos 2–5**). We were similarly able to image the hemi-brain samples from the medial side to the lateral end (**Supplementary Fig. 10** and **Supplementary Videos 6** and **7**). For Sca*l*eA2-treated adult brain samples, the sample's dorsoventral and mediolateral thickness exceeded working distance of available objective lenses (8 mm) and therefore could not be imaged in its entirety.

As a result of the limited permeability of SeeDB, large pieces of tissue, such as the full brain of adult mice, were admittedly relatively difficult to clear. This issue could be partly overcome by incubating samples at higher temperatures (for example, 50 °C), although this caused partial quenching of fluorescent proteins (SeeDB37ht; Online Methods and **Supplementary Fig. 5a**). Brain samples of younger mice (for example, P21) were easier to clear using standard protocols (**Supplementary Figs. 11** and **12** and **Supplementary Videos 8–10**).

See Developing Brain: pre-target sorting of callosal axons

SeeDB can be a powerful tool in developmental studies of embryonic and neonatal brains because of the minimal fragility and morphological damages to tissues. For example, we were able to visualize long-range callosal axon projections from one hemisphere to the other using whole-mount P7 mouse brain samples (**Fig. 4a** and

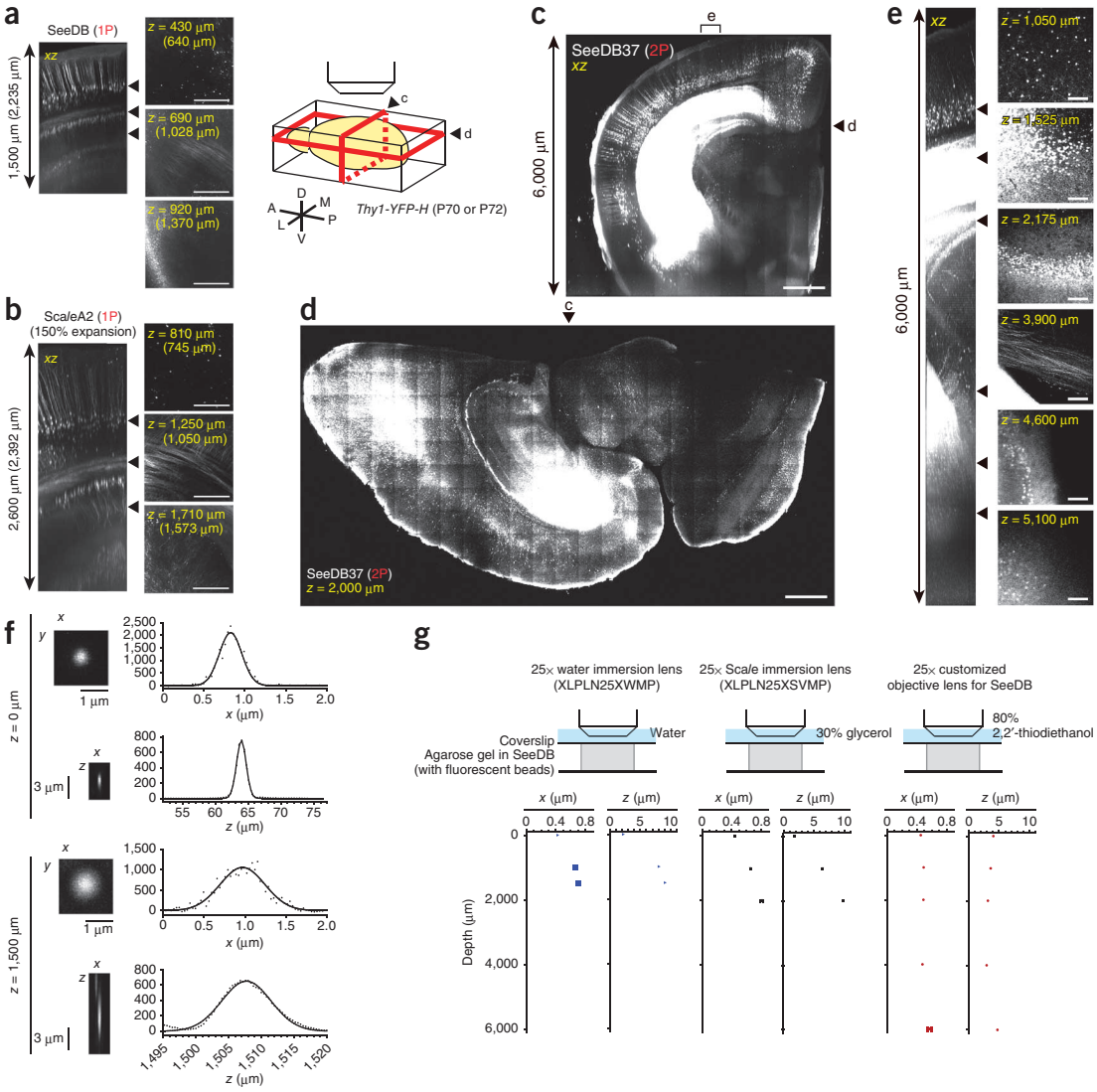

Figure 3 Fluorescence imaging of adult mouse brain. (**a**,**b**) Confocal imaging of *Thy1-YFP-H* transgenic mouse brain (P70) cleared with SeeDB (**a**) and Sca*l*eA2 (**b**). Confocal images were taken from the surface of the cerebral cortex to the hippocampus using a 10× air objective lens (Olympus, UPLSAPO10X2, NA = 0.40, working distance = 3.1 mm). Left, reconstructions along *z* axis; right, representative *xy* images (arrowheads). Because this objective lens is for non-immersion use (refractive index = 1.0), the axial scale is shortened in SeeDB (1.49) or Sca*l*eA2 (1.38) as a result of differences in refractive index. The real depth of the SeeDB-treated sample is 1,500 µm × 1.49 = 2,235 µm. Because Sca*l*eA2 induces ~150% linear expansion, the real depth of the Sca*l*eA2-treated sample is 2,600 µm/1.5 × 1.38 = 2,392 µm. Calibrated real depth in samples is shown in parentheses. Because EYFP signal intensity was weaker in Sca*l*eA2 samples, a stronger laser power was used to take the image shown in **b**. Scale bars, 500 µm. Serial confocal images for the SeeDB-treated sample are shown in **Supplementary Video 1**. (**c–e**) Two-photon imaging of adult *Thy1-YFP-H* mouse hemi-brain (P72) of ~6.0-mm-thick cleared with SeeDB37. Images were acquired from the surface of the cerebral cortex to the bottom of the brain using a customized 25× objective lens (Olympus, NA = 0.9, working distance = 8.0 mm). A, anterior; P, posterior; D, dorsal; V, ventral; M, medial; L, lateral. (**c**) An optical section along a coronal plane (indicated in schema) reconstructed from 12 × 1 blocks. Volume rendering is shown in **Supplementary Video 2**. (**d**) Images along a horizontal plane (indicated in schema, *z* = 2,000 µm from the surface) tiled and stitched (23 × 12 tiles). Serial optical sections are shown in **Supplementary Video 3**. (**e**) Images of a single *xyz* block. Left, reconstruction along *z* axis; right, representative *xy* images (arrowheads). Scale bars, 1 mm (**c**,**d**) and 100 µm (**e**). Serial section images and volume rendering are shown in **Supplementary Videos 4** and **5**, respectively. Images acquired from the medial side of the same hemi-brain sample are shown in **Supplementary Figure 10** and **Supplementary Videos 6** and **7**. (**f**) Image resolution by point-spread function analysis. Representative data for a 25× water-immersion objective lens (Olympus, XLPLN25XWMP, NA = 1.05, working distance = 2.0 mm). Fluorescence intensities along *x* and *z* axes of fluorescent microspheres (diameter = 0.5 µm) embedded in 1% agarose and equilibrated in SeeDB. Quantification is shown in **g**. (**g**) Results for three objective lenses: the 25× water-immersion objective lens, a 25× Sca*l*e-immersion objective lens (Olympus, XLPLN25XSVMP, NA = 1.0, working distance = 4.0 mm, designed for refractive index 1.38) and our customized 25× objective lens for SeeDB (Olympus, NA = 0.9, working distance = 8.0 mm, designed for refractive index 1.48, correction collar covers 1.41–1.51). Immersion media were water (refractive index = 1.33) for XLPLN25XWMP, 30% glycerol (vol/vol, refractive index = 1.38) for XLPLN25XSVMP and 80% 2,2′-thiodiethanol (vol/vol, refractive index = 1.49) for the customized objective lens. Data are full width at half maximum (FWHM). Data are mean ± s.e.m. (*n* = 8–10 beads).

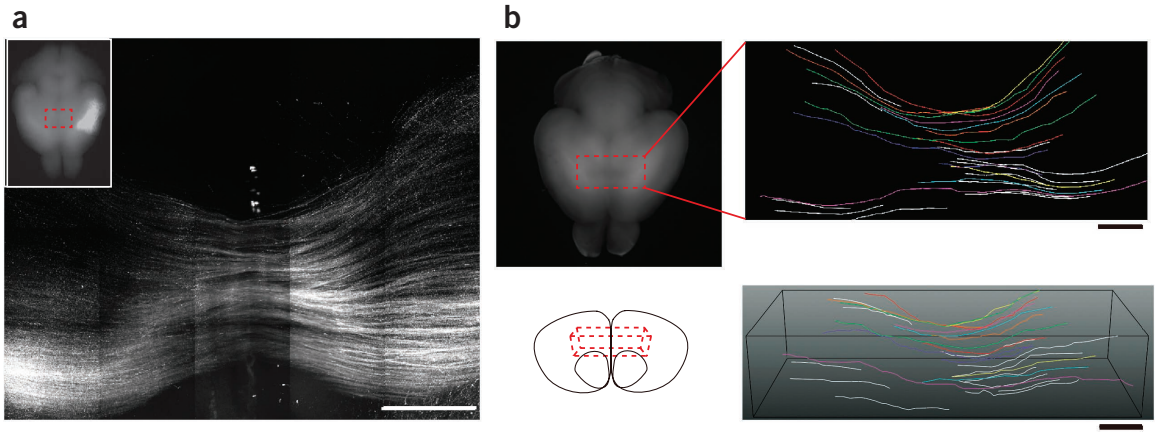

Figure 4 Topographic organization of callosal axon pathways revealed by *in utero* electroporation and optical clearing with SeeDB (SeeDBp protocol). (**a**) EGFP expression vector was electroporated into one hemisphere of the cerebral cortex at E15 and analyzed at P7. *z* stacked two-photon images (1,000 μm thick, *z* = 800–1,800 μm from the surface of the cerebral cortex) taken with a 25× objective lens (Olympus, XLPLN25XSVMP) were tiled (5 × 4 tiles). Inset in top left corner shows the epifluorescence image of the brain, and the dashed red box indicates the area imaged. Serial optical sections are shown in **Supplementary Video 11**. (**b**) Reconstruction of sparsely labeled callosal fibers. To label a small number of neurons, we co-electroporated Cre-dependent tdTomato expression vectors with a small amount of Cre expression vectors at E15 (Online Methods). *z* stacked tiled image (9 × 4 tiles, *z* = 1,500–2,500 μm) taken with our customized 25× objective lens (Olympus) is shown. A frontal view of the reconstructed callosal fibers is shown on the bottom. Plasmids were electroporated to the left hemisphere of the brain (right in figures). Dashed red boxes indicate the area imaged. Scale bars, 500 μm. Three-dimensional reconstruction of **b** is shown in **Supplementary Video 12**.

Supplementary Video 11). These mice had EGFP expression vectors introduced into layer II/III neurons in one hemisphere of the cerebral cortex at embryonic day 15 (E15) via *in utero* electroporation. Brain samples were obtained at P7 and then cleared with SeeDBp.

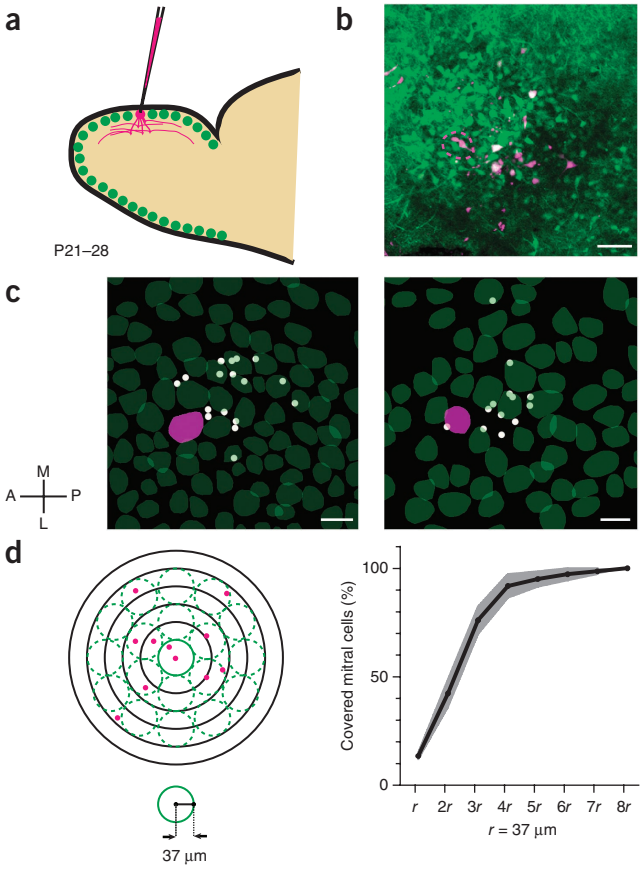

By introducing tdTomato and EGFP expression vectors to anterior and posterior regions, respectively, we were able to observe topographic organization of the corpus callosum (**Supplementary Video 12**). We also examined the fine topographic organization in axonal pathways by sparsely labeling layer II/III neurons using the *Cre-loxP* system. Single axon tracing revealed that the fine anterior-posterior layout of axons was largely, although not strictly, maintained during the course of axonal extensions across the corpus callosum, consistent with studies in human[17] (**Fig. 4b** and **Supplementary Video 13**). This result suggests that topographic callosal axon projection is ensured not only by the target-derived positional cues, but also by

Figure 5 Distribution of mitral cell somata labeled from a single glomerulus. Whole-mount olfactory bulbs were imaged from dorsal surface using confocal microscopy. (**a**) Neurons associated with a single glomerulus were labeled by electroporation of Alexa 647–dextran tracer *in vivo*. Olfactory bulb samples were then dissected and cleared with SeeDB. Confocal images were taken with a 10× air objective lens (Olympus, UPLSAPO10X2). (**b**) EYFP expression in *Thy1-YFP-G* transgenic mice was used to identify mitral cells in the olfactory bulb. In this mouse line, EYFP is expressed in mitral cells, but not in tufted cells. Neurons colabeled with dextran and EYFP were defined as sister mitral cells associated with the targeted glomerulus. A confocal image of the mitral cell layer is shown. The location of a dye-injected glomerulus is shown with a magenta broken line (*z* projected). (**c**) Distribution of sister mitral cell somata (*z*-projected images). Glomeruli in the dorsal olfactory bulb were analyzed. Two representative examples of five data sets are shown. Glomeruli are shown in green. Targeted glomerulus is shown in magenta and labeled mitral cells are shown as white dots. (**d**) Cumulative curve of sister mitral cell distribution from the centroid of these neurons (*n* = 5 glomeruli, 15.8 ± 4.3 sister mitral cells, mean ± s.d.). Data are shown as the mean ± s.d. Approximately 80% of sister mitral cells were distributed within a radius equivalent to three times the radius of the glomerulus (37 ± 10 μm, mean ± s.d., *n* = 578 glomeruli from 3 mice, age P21–28); distribution of 100% of sister mitral cells were found within a radius equal to four to seven times the radius of the glomerulus (*n* = 5 glomeruli from 5 mice, age P21–28). Thus, mitral cells that belong to a given glomerulus are highly intermingled with those of other glomeruli. Scale bars, 100 μm. A, anterior; P, posterior; M, medial; L, lateral.

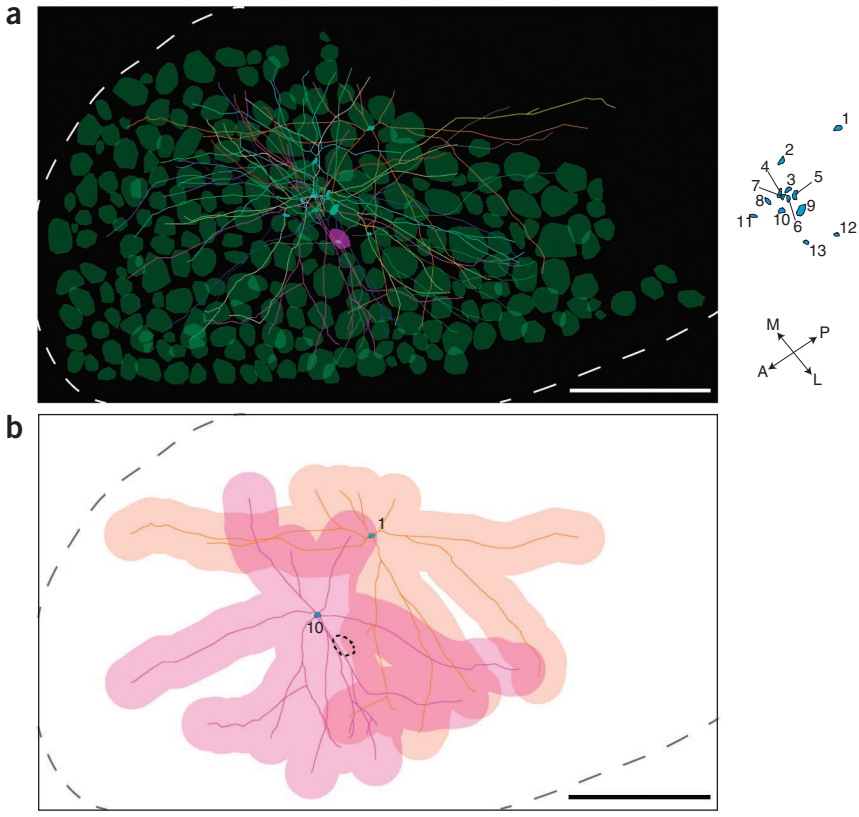

Figure 6 Tracing lateral dendrites of sister mitral cells. (**a**) *OMP-GFP* knock-in mice (P21–28) were used to trace dendrites of sister mitral cells. Distribution of lateral dendrites of sister mitral cells in one example (of three similar data sets). Primary dendrites and axons are not shown in this reconstruction. Neurons were analyzed that fit the following criteria: relatively large somata (diameter = 10–20 µm) and located in the presumptive mitral cell layer, strongly labeled with Alexa 647–dextran to allow for full tracing of lateral dendrites, >80% of lateral dendrites that were fully traced (some were interrupted by saturated signals or noise). Although external and middle tufted cells were excluded, internal tufted cells located close to the mitral cell layer may be included in our data set. All these neurons project primary dendrites to a single glomerulus shown in magenta. Other glomeruli were identified by EGFP fluorescence of *OMP-GFP* mice. Different neurons are shown in different colors. Reconstruction was based on optical sections spanning a thickness of 400 µm (in real sample). Images were taken with a confocal microscope and a 10× air objective lens (Olympus, UPLSAPO10X2). *z*-projected image is shown. Raw data (serial optical sections) are shown in **Supplementary Video 14**. (**b**) Estimated overlaps in dendrite coverage areas among sister mitral cells. The major inhibitory neurons that form synapses with lateral dendrites are granule cells. Thus, dendrite coverage area of a mitral cell was defined as the distribution area of granule cells that can potentially form synapses with a given mitral cell. Because typical granule cells extend their apical dendrites within a radius of 25–100 µm in mice, the coverage area was defined to be within 100 µm from the traced dendrites of the mitral cells[30,31]. As an example, we show overlap in coverage areas of two mitral cells, #1 and #10. Coverage area of mitral cell #1 had a 44% overlap with that of mitral cell #10. The labeled glomerulus is shown by a dotted line. Coverage areas of 13 sister mitral cells in **a** were determined on the basis of *z*-projected images and are shown in **Supplementary Figure 13**. Percentages of shared coverage areas were determined for all 144 pairs of sister mitral cells (37 ± 20%, mean ± s.d., n = 144 pairs; **Supplementary Table 3**). Scale bars, 500 µm.

pre-target axon sorting[18,19]. In combination with genetic manipulations, our methods should facilitate efforts to understand the molecular mechanisms underlying long-range axonal projection in the brain.

Non-conserved dendrite wiring among sister mitral cells

SeeDB is also ideal for use in comprehensive and quantitative reconstruction of microcircuits in the brain. We used our clearing method to examine the anatomical bases for odor information processing in a single glomerular module in the olfactory bulb. In the mouse olfactory system, olfactory sensory neurons expressing a given type of odorant receptor converge their axons to a pair of glomeruli in the olfactory bulb. Odor inputs to a single glomerulus are then relayed to 20–50 mitral and tufted cells through their primary dendrites. Each mitral/tufted cell has a single primary dendrite and several lateral dendrites. Although primary dendrites of mitral/tufted cells receive inputs from a single glomerulus, lateral dendrites form reciprocal synapses with inhibitory granule cells and receive inputs from other glomerular modules and centrifugal fibers. 'Sister' mitral cells connecting to the same glomerulus receive common excitatory inputs as a result of electrical coupling and glutamate spill over in the glomerulus[20]; however, the extent of the diversity in the inhibitory modulations via lateral dendrites among sister mitral cells remains unknown[21].

To label neurons associated with a single glomerulus, we electroporated fluorescence-labeled dextran tracers into a single glomerulus on the dorsal surface of the olfactory bulb using a glass pipette (**Fig. 5a**)[22]. *OMP-GFP* knock-in mice or *Thy1-YFP* line G transgenic mice were used to visualize glomerular structures and/or mitral cells[16,23]. After optical clearing with SeeDB, the whole-mount olfactory bulb samples were imaged using confocal microscopy. A subsequent quantitative analysis was performed only when labeled mitral cells in a sample were all found to be associated with a single glomerulus.

We first analyzed the distribution of sister mitral cell somata. Various types of neurons were labeled by the tracer, but the mitral cells were identified by the expression of the *Thy1-YFP-G* transgene (**Fig. 5b**). We found 15.8 ± 4.3 labeled mitral cells per glomerulus (mean ± s.d., n = 5 glomeruli). The tracer-labeled mitral cells were widespread in an area much larger than the size of a single glomerulus: sister mitral cells were distributed in an area with a 4–7-fold larger radius (n = 5 glomeruli) than the average radius of a glomerulus (37 ± 10 µm, mean ± s.d., n = 578 glomeruli from 3 mice at P21–28) (**Fig. 5c,d**). Thus, somata of sister mitral cells are highly intermingled with non-sister mitral cells.

Next, we compared the lateral dendrite patterns among sister mitral cells. Because lateral dendrites are spread over a large area in the olfactory bulb, comprehensive reconstruction has been extremely laborious and difficult using the serial mechanical sectioning approach, even for a single neuron[24–27]. The whole-mount olfactory bulb sample was too thick even with two-photon microscopy[28,29], but, after optical clearing of this sample with SeeDB, we were able to visualize the near-complete wiring diagram of mitral cell dendrites using confocal microscopy (**Fig. 6a**

and **Supplementary Video 14**). On the basis of this tracing data, we quantified various parameters of mitral cell dendrites (**Supplementary Table 2**). We defined the coverage area for a mitral cell as the area within 100 µm of the mitral cell dendrites (**Supplementary Fig. 13**) because its major synaptic partners, granule cells, are known to extend their dendrites in this range (within a radius of 25–100 µm)[30,31]. Under this assumption, we found that the coverage areas of sister mitral cells only have small overlapping areas (mean ± s.d. = 37 ± 30%, n = 144 pairs; **Fig. 6b** and **Supplementary Table 3**). As these coverage areas are maximum estimates, they are likely to be overestimated: many granule cells extend dendrites to smaller areas (<100 µm), not all granule cells form synapses with lateral dendrites passing through this area and functional synapses seem to be more localized[30,32]. Thus, our results support the idea that synaptic partners (granule cells) are highly diverse among sister mitral cells.

DISCUSSION

We developed SeeDB, a new water-based optical clearing agent that contains fructose and α-thioglycerol and is compatible with various fluorescent proteins and neuronal tracers. Compared with Sca*l*e, a previously established aqueous clearing solution, our method is quicker and minimizes morphological distortions and fragility to tissues while maintaining a comparable level of clarity. A recently reported clearing technique, CLARITY, is advantageous for antibody staining of thick samples, but it requires complicated procedures[33]. Because our protocol is quick, easy, inexpensive, safe and requires no special equipment, SeeDB could prove useful for a broad range of researchers working in neuroscience and developmental biology (**Supplementary Table 4**). A notable feature of SeeDB is its compatibility with lipophilic dyes, such as DiI, which can be used for neuronal tracing of post-fixed brains (**Fig. 2e**). This means that SeeDB could be applied to study neuronal circuits in non-transgenic species, including human samples.

SeeDB is particularly advantageous for quantitative analyses of fine neuronal morphology and microcircuits because minimal deformation artifacts occur during the clearing process. Indeed, in the olfactory bulb, the morphology of mitral cells observed after the clearing was indistinguishable to that observed *in vivo* (**Fig. 2a**,**b**). Using the SeeDB-cleared samples, we were able to construct a near-complete wiring diagram of mitral cells associated with a single glomerulus (**Fig. 6**).

Although odor information in a single glomerulus is relayed to multiple mitral cells, there is controversy regarding the extent to which odor information processing is conserved among the sister mitral cells. In one scenario, sister mitral cells may encode similar and redundant odor information and send parallel and robust outputs. In *Drosophila*, sister projection neurons (equivalent to mammalian mitral cells) receive highly synchronous excitatory inputs and their axonal projection patterns are relatively stereotyped[34]. Similarly, in *Xenopus*, sister mitral/tufted cells receive highly synchronous odor inputs[35]. In the rodent olfactory bulb, however, inhibitory neurons outnumber mitral cells by >100-fold[36,37]. Recent studies have demonstrated the variability in odor information coding among sister mitral cells[38,39]. We found that somata of mitral cells belonging to a common glomerular module were highly intermingled with those of surrounding glomeruli (**Fig. 5**). Long lateral dendrites sparsely covered the olfactory bulb, consistent with reports from earlier tracing experiments[24,27,30] and electrophysiological studies[32]. Furthermore, the pattern of lateral dendrites were not conserved among sister mitral cells (**Fig. 6**). Thus, lateral connectivity is not strictly center-surround, and sister mitral cells are likely differentially tuned by inhibitory granule cells, thereby encoding odor information in different temporal kinetics and tuning specificities. In addition, recent studies have shown that axonal projection patterns are also diverse among sister mitral cells, at least in the piriform cortex[25,28,29,40,41]. Thus, sister mitral cells may send divergent odor information to different sets of target neurons in the olfactory cortex.

Recent studies in the visual cortex have reported that daughter neurons produced from a common progenitor cell are preferentially recruited to a common microcircuit and share a visual selectivity[42–44]. In the olfactory bulb, developmental origins of mitral/tufted cells associated with a common glomerulus still remain undetermined. Deciphering odor coding strategy by a single glomerular module and its developmental mechanisms are important ongoing issues in the olfactory system. As we demonstrated in the olfactory bulb, our optical clearing method should facilitate studies incorporating light microscopy–based connectomics and complement the recent developments in genetic neural circuit tracing techniques, such as Brainbow[45], retrograde-anterograde trans-synaptic labeling[46,47] and synapse labeling[48].

METHODS

Methods and any associated references are available in the online version of the paper.

Note: Supplementary information is available in the online version of the paper.

ACKNOWLEDGMENTS

We thank J.R. Sanes (Harvard) (*Thy1-YFP-G*, *H*) and P. Mombaerts (Max Planck Institute) (*OMP-GFP*) for providing mouse strains. We are also grateful to M. Eiraku and K. Muguruma for assistance with two-photon microscopy setup, Olympus for the customized objective lens, Y. Mimori-Kiyosue for equipment, J. Nabekura and T. Nemoto for instructions on *in vivo* two-photon imaging, and R. Iwata and H. Hiraga for valuable comments on the manuscript. This work was supported by grants from the PRESTO program of the Japan Science and Technology Agency, the Sumitomo Foundation, the Nakajima Foundation, the Mitsubishi Foundation, the Strategic Programs for R&D (President's Discretionary Fund) of RIKEN, and the Ministry of Education, Culture, Sports, Science and Technology (MEXT) of Japan (to T.I.). The imaging experiments were supported by the RIKEN Center for Developmental Biology Imaging Facility and the Four-dimensional Tissue Analysis Unit. Animal experiments were supported by the Laboratory for Animal Resources and Genetic Engineering at the RIKEN Center for Developmental Biology.

AUTHOR CONTRIBUTIONS

M.-T.K. performed most of the experiments. S.F. performed *in utero* electroporation. T.I. conceived the experiments, performed the initial phase of experiments, supervised the project and wrote the manuscript.

COMPETING FINANCIAL INTERESTS

The authors declare competing financial interests: details are available in the online version of the paper.

1. Tsai, P.S. *et al.* Correlations of neuronal and microvascular densities in murine cortex revealed by direct counting and colocalization of nuclei and vessels. *J. Neurosci.* **29**, 14553–14570 (2009).
2. Helmchen, F. & Denk, W. Deep tissue two-photon microscopy. *Nat. Methods* **2**, 932–940 (2005).
3. Tuchin, V. *Tissue Optics: Light Scattering Methods and Instruments for Medical Diagnosis*, 2nd edn. (SPIE Press, 2007).
4. Dent, J.A., Polson, A.G. & Klymkowsky, M.W. A whole-mount immunocytochemical analysis of the expression of the intermediate filament protein vimentin in *Xenopus*. *Development* **105**, 61–74 (1989).
5. Dodt, H.U. *et al.* Ultramicroscopy: three-dimensional visualization of neuronal networks in the whole mouse brain. *Nat. Methods* **4**, 331–336 (2007).
6. Staudt, T., Lang, M.C., Medda, R., Engelhardt, J. & Hell, S.W. 2,2′-thiodiethanol: a new water soluble mounting medium for high resolution optical microscopy. *Microsc. Res. Tech.* **70**, 1–9 (2007).
7. Gonzalez-Bellido, P.T. & Wardill, T.J. Labeling and confocal imaging of neurons in thick invertebrate tissue samples. *Cold Spring Harb. Protoc.* published online, http://dx.doi.org/doi:10.1101/pdb.prot069625 (1 September 2012).

8. Becker, K., Jahrling, N., Saghafi, S., Weiler, R. & Dodt, H.U. Chemical clearing and dehydration of GFP expressing mouse brains. *PLoS ONE* **7**, e33916 (2012).
9. Ertürk, A. *et al.* Three-dimensional imaging of the unsectioned adult spinal cord to assess axon regeneration and glial responses after injury. *Nat. Med.* **18**, 166–171 (2012).
10. Taylor, W.R. An enzyme method of clearing and staining small vertebrates. *Proc. USA Natl. Museum* **122**, 1–17 (1967).
11. Dingerkus, G. & Uhler, L.D. Enzyme clearing of alcian blue stained whole small vertebrates for demonstration of cartilage. *Stain Technol.* **52**, 229–232 (1977).
12. Hama, H. *et al.* Scale: a chemical approach for fluorescence imaging and reconstruction of transparent mouse brain. *Nat. Neurosci.* **14**, 1481–1488 (2011).
13. Klymkowsky, M.W. & Hanken, J. Whole-mount staining of *Xenopus* and other vertebrates. *Methods Cell Biol.* **36**, 419–441 (1991).
14. Bancroft, J.D. & Gamble, M. *Theory and Practice of Histological Techniques* (Churchill Livingstone, 2007).
15. Dills, W.L. Jr. Protein fructosylation: fructose and the Maillard reaction. *Am. J. Clin. Nutr.* **58**, 779S–787S (1993).
16. Feng, G. *et al.* Imaging neuronal subsets in transgenic mice expressing multiple spectral variants of GFP. *Neuron* **28**, 41–51 (2000).
17. Hofer, S. & Frahm, J. Topography of the human corpus callosum revisited–comprehensive fiber tractography using diffusion tensor magnetic resonance imaging. *Neuroimage* **32**, 989–994 (2006).
18. Imai, T. *et al.* Pre-target axon sorting establishes the neural map topography. *Science* **325**, 585–590 (2009).
19. Nishikimi, M., Oishi, K., Tabata, H., Torii, K. & Nakajima, K. Segregation and pathfinding of callosal axons through EphA3 signaling. *J. Neurosci.* **31**, 16251–16260 (2011).
20. Schoppa, N.E. & Westbrook, G.L. Glomerulus-specific synchronization of mitral cells in the olfactory bulb. *Neuron* **31**, 639–651 (2001).
21. Murthy, V.N. Olfactory maps in the brain. *Annu. Rev. Neurosci.* **34**, 233–258 (2011).
22. Nagayama, S. *et al. In vivo* simultaneous tracing and Ca^{2+} imaging of local neuronal circuits. *Neuron* **53**, 789–803 (2007).
23. Potter, S.M. *et al.* Structure and emergence of specific olfactory glomeruli in the mouse. *J. Neurosci.* **21**, 9713–9723 (2001).
24. Orona, E., Rainer, E.C. & Scott, J.W. Dendritic and axonal organization of mitral and tufted cells in the rat olfactory bulb. *J. Comp. Neurol.* **226**, 346–356 (1984).
25. Ghosh, S. *et al.* Sensory maps in the olfactory cortex defined by long-range viral tracing of single neurons. *Nature* **472**, 217–220 (2011).
26. Igarashi, K.M. *et al.* Parallel mitral and tufted cell pathways route distinct odor information to different targets in the olfactory cortex. *J. Neurosci.* **32**, 7970–7985 (2012).
27. Mori, K., Kishi, K. & Ojima, H. Distribution of dendrites of mitral, displaced mitral, tufted, and granule cells in the rabbit olfactory bulb. *J. Comp. Neurol.* **219**, 339–355 (1983).
28. Nagayama, S. *et al.* Differential axonal projection of mitral and tufted cells in the mouse main olfactory system. *Front. Neural Circuits* **4**, 120 (2010).
29. Sosulski, D.L., Bloom, M.L., Cutforth, T., Axel, R. & Datta, S.R. Distinct representations of olfactory information in different cortical centres. *Nature* **472**, 213–216 (2011).
30. Kim, D.H. *et al.* Lateral connectivity in the olfactory bulb is sparse and segregated. *Front. Neural Circuits* **5**, 5 (2011).
31. Orona, E., Scott, J.W. & Rainer, E.C. Different granule cell populations innervate superficial and deep regions of the external plexiform layer in rat olfactory bulb. *J. Comp. Neurol.* **217**, 227–237 (1983).
32. Fantana, A.L., Soucy, E.R. & Meister, M. Rat olfactory bulb mitral cells receive sparse glomerular inputs. *Neuron* **59**, 802–814 (2008).
33. Chung, K. *et al.* Structural and molecular interrogation of intact biological systems. *Nature* **497**, 332–337 (2013).
34. Kazama, H. & Wilson, R.I. Origins of correlated activity in an olfactory circuit. *Nat. Neurosci.* **12**, 1136–1144 (2009).
35. Chen, T.W., Lin, B.J. & Schild, D. Odor coding by modules of coherent mitral/tufted cells in the vertebrate olfactory bulb. *Proc. Natl. Acad. Sci. USA* **106**, 2401–2406 (2009).
36. Kaplan, M.S., McNelly, N.A. & Hinds, J.W. Population dynamics of adult-formed granule neurons of the rat olfactory bulb. *J. Comp. Neurol.* **239**, 117–125 (1985).
37. Hinds, J.W. & McNelly, N.A. Aging of the rat olfactory bulb: growth and atrophy of constituent layers and changes in size and number of mitral cells. *J. Comp. Neurol.* **72**, 345–367 (1977).
38. Dhawale, A.K., Hagiwara, A., Bhalla, U.S., Murthy, V.N. & Albeanu, D.F. Non-redundant odor coding by sister mitral cells revealed by light addressable glomeruli in the mouse. *Nat. Neurosci.* **13**, 1404–1412 (2010).
39. Kikuta, S., Fletcher, M.L., Homma, R., Yamasoba, T. & Nagayama, S. Odorant response properties of individual neurons in an olfactory glomerular module. *Neuron* **77**, 1122–1135 (2013).
40. Miyasaka, N. *et al.* From the olfactory bulb to higher brain centers: genetic visualization of secondary olfactory pathways in zebrafish. *J. Neurosci.* **29**, 4756–4767 (2009).
41. Miyamichi, K. *et al.* Cortical representations of olfactory input by trans-synaptic tracing. *Nature* **472**, 191–196 (2011).
42. Yu, Y.C. *et al.* Preferential electrical coupling regulates neocortical lineage-dependent microcircuit assembly. *Nature* **486**, 113–117 (2012).
43. Li, Y. *et al.* Clonally related visual cortical neurons show similar stimulus feature selectivity. *Nature* **486**, 118–121 (2012).
44. Ohtsuki, G. *et al.* Similarity of visual selectivity among clonally related neurons in visual cortex. *Neuron* **75**, 65–72 (2012).
45. Livet, J. *et al.* Transgenic strategies for combinatorial expression of fluorescent proteins in the nervous system. *Nature* **450**, 56–62 (2007).
46. Marshel, J.H., Mori, T., Nielsen, K.J. & Callaway, E.M. Targeting single neuronal networks for gene expression and cell labeling *in vivo*. *Neuron* **67**, 562–574 (2010).
47. Lo, L. & Anderson, D.J.A. Cre-dependent, anterograde transsynaptic viral tracer for mapping output pathways of genetically marked neurons. *Neuron* **72**, 938–950 (2011).
48. Kim, J. *et al.* mGRASP enables mapping mammalian synaptic connectivity with light microscopy. *Nat. Methods* **9**, 96–102 (2012).

ONLINE METHODS

Reagents. Reagents were purchased from Nacalai Tesque, Tokyo Kasei or Wako Chemicals. To prepare fructose solutions, D(−)-fructose was dissolved completely in distilled H_2O at 65 °C. After cooling to 25 °C or 37 °C, α-thioglycerol was added to give a final concentration of 0.5%. SeeDB (80.2% (wt/wt) fructose; ~115%, wt/vol) or SeeDB37 (86.7% (wt/wt) fructose; ~130%, wt/vol) solutions were prepared on the basis of percent weight/weight to ensure accuracy. Other fructose solutions (20–100%, wt/vol) were prepared on the basis of percent weight/volume. Refractive indices were determined at 25 °C using an Abbe refractometer (Erma) with a white LED light source.

Mice. All animal experiments were approved by the Animal Experiment Committee of the RIKEN Kobe Institute. Wild-type (C57BL/6N) and *Thy1-YFP* (line G and H)[16] mice in C57BL/6N background (both males and females) were used for optical clearing. *Thy1-YFP-G* mouse lines were used to evaluate stability of fluorescent proteins. ICR mice were used for *in utero* electroporation. Mice were deeply anesthetized with an overdose of Nembutal (Dainippon Sumitomo Pharma), and killed by intracardiac perfusion with PBS. Excised brains or embryos were fixed with 4% (wt/vol) paraformaldehyde (PFA) in PBS at 4 °C overnight. Brain slices were prepared using a microslicer (Dosaka EM).

Optical clearing using SeeDB. For some imaging experiments, fixed samples were first embedded into 1% agarose (Invitrogen, UltraPure Agarose) in PBS. For clearing, fixed samples were serially incubated in 20–30 ml of 20%, 40% and 60% (wt/vol) fructose, each for 4–8 h in 50-ml conical tubes with gentle shaking (~17 r.p.m., for slices) or rotation (~4 r.p.m., for whole-mount samples) at 25 °C. Samples were then incubated in 80% (wt/vol) fructose for 12 h, 100% (wt/vol) fructose for 12 h and finally in SeeDB (80.2% wt/wt fructose) for 24 h with gentle shaking or rotation at 25 °C. The concentration of fructose could be increased up to 86.7% (wt/wt, SeeDB37) when clearing was performed at 37 °C. When samples showed volume expansion under the above conditions (for example, neonatal brain samples), 20–80% fructose solutions were prepared with 0.1× PBS instead of H_2O (SeeDBp). All fructose solutions contained 0.5% α-thioglycerol. **Supplementary Figure 5a** summarizes the incubation schedules of these protocols. Large tissue samples require longer incubation times due to the viscosity of SeeDB. For example, adult whole-brain samples were more difficult to clear than hemi-brain samples. Agarose-embedded samples also typically required longer incubation times for efficient clearing. We recommend trimming the samples to the minimal size needed for an experiment to allow efficient penetration of SeeDB. Penetration efficiency can also be improved by clearing tissues at higher temperatures (for example, 50 °C) because higher temperatures reduce viscosity of SeeDB. In the high temperature protocol (SeeDB37ht), clearing was performed at 50 °C as follows: 3 h each in 20%, 40%, 60% and 80% (wt/vol) fructose, 12 h in 100% (wt/vol) fructose, 24 h in SeeDB, and 24 h in SeeDB37. Incubation at higher temperatures may cause mild sample expansion and partial quenching of fluorescent proteins. Thus, optimal conditions should be determined on the basis of desired clarity, accumulation of autofluorescence and stability of fluorescent dyes. Samples can be stored in SeeDB (at 25 °C) or SeeDB37 (at 37 °C) for up to 1 week.

Optical clearing with Sca*l*eA2 and Sca*l*eU2 (ref. 12). Fixed samples were transferred to an excess volume of Sca*l*eA2 (4 M urea, 10% (wt/vol) glycerol, and 0.1% (vol/vol) Triton X-100) or Sca*l*eU2 (4 M urea, 30% glycerol, and 0.1% Triton X-100)[12] and incubated at 25 °C with gentle shaking for 21 d.

Optical clearing with sucrose[1]. Fixed samples were incubated in 2% Triton X-100 in PBS for 24 h. Samples were then serially incubated in 15%, 30%, 45% and 60% sucrose in 2% Triton X-100–PBS.

Optical clearing with BABB[5]. Fixed samples were serially incubated in 50%, 80% and 100% ethanol, each for 8 h. Next, they were incubated in 100% ethanol for 12 h, and further placed in hexane for 12 h. Finally, the samples were incubated in BABB solution (benzyl alcohol:benzyl benzoate = 1:2) with gentle shaking for 24 h.

Optical clearing with dibenzyl ether[8]. Fixed samples were serially incubated in 50%, 80% and 100% tetrahydrofuran, each for 8 h. This was followed by two 12-h incubations in 100% tetrahydrofuran. Samples were then cleared in dibenzyl ether with gentle shaking for 24 h.

Measurement of light transmittance. Light transmittance of clearing agents and cleared brain tissues was determined using a spectrophotometer (Beckman DU730). The light scattering of adult brain was non-homogeneous as a result of the presence of myelinated structures; thus, we used P21 mouse hemi-brains for transmittance measurements. Because sample expansion alone can reduce light scattering, we used samples with a defined thickness (5.13 ± 0.19 mm, mean ± s.d., $n = 3$) for clearing and then compared their transmittance values.

Measurement of sample size changes. For the measurement of sample expansion and shrinkage, the mouse brain samples (P3 or P21) were cut along the midline, and hemi-forebrains were excised. Photos were taken of samples placed on a glass dish with the midplane on the bottom. Based on top view photos, the area of the midplane was determined using MetaMorph software (Molecular Devices). The linear expansion value was determined by the square root of the area size changes.

Two-photon imaging using an upright microscope. For imaging agarose-embedded SeeDB-cleared brain samples, the agarose block was trimmed and the sample was placed on a Petri dish (**Supplementary Fig. 5b**,**c**). Non-embedded samples were placed in a hand-made chamber with SeeDB (**Supplementary Fig. 5d**). A coverslip or a custom-made glass-bottomed Petri dish was placed on top of it, and H_2O (for UMPLFLN 10XW and XLPLN25XWMP), 30% glycerol (plus H_2O, vol/vol, refractive index = 1.38; for XLPLN25XSVMP), 80% 2,2′-thiodiethanol (plus H_2O, vol/vol, refractive index = 1.49, for a 25× customized objective lens), or 90% 2,2′-thiodiethanol (refractive index = 1.50, for imaging SeeDB37-cleared samples with the customized objective lens) were used for immersion. SeeDB should not be used directly for immersion; its viscosity causes an uneven refraction index distribution after evaporation of water from the surface of SeeDB during imaging and can impair image quality. Samples cleared with SeeDB37 were incubated at 37 °C using a thermo plate (Tokai Hit) during imaging. For imaging Sca*l*eA2-treated samples, the samples were placed on the bottom of a plastic dish in 0.3% agarose and Sca*l*eA2 was used for immersion. An upright multiphoton microscope (Olympus, FV1000MPE) was used for two-photon imaging. A 10× objective lens (Olympus, UMPLFLN 10XW, NA = 0.30, working distance = 3.3 mm, water immersion), a 25× objective lens (Olympus, XLPLN25XWMP, NA = 1.05, working distance = 2.0 mm, water immersion), a 25× objective lens (Olympus, XLPLN25XSVMP, NA = 1.0, working distance = 4.0 mm, designed for refractive index 1.38), a 25× objective lens (Olympus, XLSLPLN25XSVMP, NA = 0.9, working distance = 8.0 mm, designed for refractive index 1.38) or a customized 25× objective lens (Olympus, NA = 0.9, working distance = 8.0 mm, designed for refractive index 1.48, correction collar covers 1.41 to 1.51) was used for imaging. MaiTai DeepSee (Spectra-Physics) or InSight DeepSee Dual (Spectra-Physics) was used for two-photon excitation of EYFP at 920 or 950 nm, respectively. EGFP and tdTomato were excited at 920 and 1,040 nm, respectively, using InSight DeepSee Dual. Fluorescence signals were quantified with a non-descanned GaAsP PMT. For the 25× objective lenses, correction collars were used to achieve best brightness and resolution. Laser power was manually adjusted to give constant fluorescence intensities at all depths. Imaging and stitching of tiled images were carried out with a motorized stage (Sigma Koki) and Fluoview FV10-ASW software (Olympus). For visualizing projection images and three-dimensional reconstructions, Neurolucida software (MBF Bioscience) was used. Objective lenses used in this study and imaging conditions for all figures are summarized in **Supplementary Table 5**.

Point-spread-function analysis. Fluorescent microspheres (yellow-green fluorescent FluoSpheres, diameter = 0.5 µm, Invitrogen) were embedded in 1% agarose and the agarose block was equilibrated in SeeDB as described above. Two-photon *xyz* images of fluorescent beads at different depths were acquired at 920-nm excitation, as above. Gaussian fitting was used to obtain the full width at half-maximum (FWHM) values for *x* and *z* axes. The FWHM was given as 2.355σ after Gaussian fitting.

Confocal imaging using an inverted microscope. The cleared brain was dipped in a hand-made glass-bottomed chamber filled with SeeDB, Sca*l*eA2,

BABB or dibenzyl ether. Confocal images were taken with an inverted confocal microscope (Olympus, FV1000 built on IX81). Images were taken with 4× (Olympus, UPLSAPO 4X, NA = 0.16, working distance = 13 mm), 10× (Olympus, UPLSAPO10X2, NA = 0.40, working distance = 3.1 mm) or 20× (Olympus, UPLSAPO20X, NA = 0.75, working distance = 0.6 mm) objectives. A He-Ne laser (633 nm) was used for visualizing Alexa Fluor 647–dextran. EYFP was visualized with an Ar laser (488 nm). AlexaFluor 647 and DAPI were visualized with a He-Ne laser (633 nm) and an LD 405-nm laser, respectively.

***In vivo* electroporation of fluorescent dextran dyes.** Tracer electroporation was performed as described previously[22]. For single-glomerulus labeling, *OMP-GFP*[23] or *Thy1-YFP-G*[16] mice were used. Mice (P21–28) were injected with Nembutal (Dainippon Sumitomo Pharma, 50 mg per kg of body weight), RIMADYL (Pfizer) and Dexamethasone (Kyoritsu Seiyaku). Anesthetized mice were kept on a heating pad set at 35 °C. The skull overlying the dorsal olfactory bulb was carefully removed keeping the dura mater intact. A pulled glass pipette (outer tip diameter = 5–10 μm) was backfilled with AlexaFluor 488– or AlexaFluor 647–dextran (10 kDa, Invitrogen) diluted in PBS at 0.5%. Under a fluorescence stereomicroscope (Leica M205C), the pipette was moved into the glomerular layer of the olfactory bulb using a micromanipulator (Narishige). Pulsed positive current (1 μA, 0.5 s ON / 1.5 s OFF cycle) was applied for 3–5 min using an iontophoresis current generator (Stoelting). After current injection, the dura was overlaid with Kwik-Sil (WPI) and sealed with a coverslip. The mice were analyzed 3 h later by *in vivo* two-photon imaging and/or killed for optical clearing.

***In vivo* two-photon imaging.** Anesthetized mice were head-fixed under a microscope. An upright multiphoton microscope (Olympus, FV1000MPE) was used for imaging with a water-immersion 25× objective lens (Olympus, XLPLN25XWMP, NA = 1.05, working distance = 2.0). AlexaFluor 488–dextran was excited at 920 nm using MaiTai DeepSee (Spectra-Physics).

Reconstruction of mitral cell dendrites. Confocal images of mitral cells were analyzed using Neurolucida software (MBF Bioscience). Dendrites were manually traced in three-dimensional space. To quantify coverage area of a mitral cell, the *z*-projected images were analyzed. Coverage area was defined as the area within a distance of 100 μm from lateral dendrites of a mitral cell. Overlapping areas were quantified using Metamorph software (Molecular Devices). To determine the radius of a glomerulus, we first measured its perimeter in *z*-projected images. The radius was given as perimeter/2π.

DiI labeling. Excised mouse brain samples (P5 and P7) were fixed with 4% PFA in PBS at 4 °C overnight. DiI labeling was performed as described previously[49]. A small incision was made with a scalpel in the lateral olfactory tract, and a small DiI C_{18} (3) crystal (Invitrogen) was placed into the incision. The brain sample was then incubated in 2% or 4% PFA in PBS at 37 °C for 5–21 d. The samples were then cleared with SeeDB. Cleared whole-mount samples were imaged using an inverted confocal microscope (Olympus, FV1000) with a He-Ne laser (543 nm).

***In utero* electroporation.** *pCAG-EGFP* or *pCAG-tdTomato* vector (2 μg μl^{-1}) was used for *in utero* electroporation to label callosal axons. *pCAG-loxP-Neo-loxP-EYFP* or *pCAG-loxP-Neo-loxP-tdTomato* (3 μg μl^{-1}) and *pCAG-Cre* (20 ng μl^{-1}) were co-electroporated to sparsely label the callosal projection neurons. To evaluate stability of fluorescent proteins, *pCAG-ECFP/EGFP/EYFP/tdTomato* were electroporated into the cerebral cortex. *In utero* electroporation was performed as described previously[50]. Pregnant ICR mice were anesthetized with Nembutal and the uterine horns carrying embryos were exposed through a midline abdominal incision. At E15, 1 μl of plasmid solutions diluted in PBS were injected into the lateral ventricle of the embryos using a micropipette made from a glass capillary. Subsequently, electric pulses (single 10-ms poration pulse at 72–75 V, followed by five 50-ms driving pulses at 34–36 V with 950-ms intervals) were delivered with forceps-type electrodes (5-mm diameter, BEX) and a CUY21EX electroporator (BEX). The uterine horns were then placed back into the abdominal cavity before suturing the abdominal wall and skin. Electroporated mice developed normally and were dissected at P7. FastGreen is commonly used to visualize DNA solutions for *in utero* electroporation, but it caused strong background fluorescence after SeeDB treatment, hindering fluorescence imaging. We therefore used 0.05% AlexaFluor 647–dextran (10 kDa, Invitrogen) to visualize DNA solutions in blue, when necessary.

Immunohistochemistry of sections. Brain samples cleared with Sca*l*eA2 were restored in PBS overnight and then post-fixed in 4% PFA in PBS overnight. Samples cleared with SeeDB were serially incubated in 80%, 60%, 40% and 20% fructose, each for 8 h, and then in PBS overnight. Restored samples were cryoprotected with 30% sucrose overnight and embedded in OCT compound (Sakura). Coronal sections (20 μm thick) were cut with a cryostat (Leica). Cryostat sections were fixed with 4% PFA in PBS for 15 min. Sections were then blocked with 2% donkey serum for 1 h and then incubated with rabbit antibody to gephyrin (Abcam, ab25784) at 1:100, mouse antibody to gephyrin (mAb7a, Synaptic Systems, #147 021) at 1:100 or with mouse antibody to MAP2 (Sigma, M9942) at 1:200 overnight at 4 °C. After three washes with PBS, sections were incubated with Alexa 647–conjugated secondary antibodies (Invitrogen, A31573 and A31571) at 1:250 for 1 h. DAPI was used for nuclear counterstaining. Images were acquired with a confocal microscope (Olympus, FV1000). All of the antibodies used have previously been verified by the manufacturers for use in immunohistochemistry of mouse frozen sections, and the data are reported on the manufacturers' datasheet.

Whole-mount immunohistochemistry. Dissected brain samples of P28-35 *OMP-GFP* knock-in mice were fixed in 4% PFA overnight. Samples were then permeabilized in 10% BSA in PBST (1% Triton-X 100 in PBS) overnight at 4 °C. Next, the samples were incubated with chicken antibody to tyrosine hydroxylase (Abcam, ab76442, 1:250) in 10% BSA in PBST for 48 h at 4 °C. After three successive 30-min washes in PBST, samples were incubated with Alexa 647–conjugated goat antibody to chicken (Invitrogen, A21449, 1:250) in 10% BSA in PBST for 24 h at 4 °C. Samples were then washed three times in PBST. Finally, the samples were cleared with SeeDB and imaged using confocal microscopy. The antibody to tyrosine hydroxylase antibody has been verified by the manufacturer for use in immunohistochemistry of mouse frozen sections (available on the datasheet). The staining pattern of our whole-mount immunohistochemistry was consistent with our results of frozen sections (data not shown).

Quantification of fluorescence intensities of brain sections. To evaluate stability of fluorescent proteins in tissues, we used brain sections of *Thy1-YFP-G* mouse line and mice electroporated with fluorescent proteins (ECFP, EGFP, EYFP and tdTomato). Cryosections (20 μm thick) on glass slides were fixed with 4% PFA in PBS for 15 min and rinsed in PBS. Cryostat sections were then incubated in various optical clearing agents at 25 °C. For BABB and dibenzyl ether, sections were air-dried before incubation. An inverted fluorescent microscope (Leica, DMI6000B) with a cooled CCD camera was used to evaluate quenching of fluorescent proteins in the clearing agents. The sections were imaged in the same area over a period of time. Fluorescence intensity was standardized to intensity in PBS (100%).

Statistical analysis. All the experiments were performed at least three times with similar results. When quantitative data for a single representative experiment is shown, the number of experiments that was performed is specified in figure legends (**Fig. 2d**, **5**, **6**, **Supplementary Fig. 6**). The data shown in **Figures 1d**,**e**,**g**, **2d** and **3g**, and **Supplementary Figures 4** and **6** are technical replicates. Sample sizes for technical replicates were 3–10 (specified in figure legends) because s.e.m. (reported for each result) in these experiments are much smaller than the differences among different conditions. The data shown in **Figures 5** and **6**, and **Supplementary Tables 2** and **3** are biological replicates and sample sizes were determined by the nature of samples and the number of mice used (3–5). The numbers of mice used were sufficient to confirm reproducibility. Prism5 software (GraphPad) was used for statistical analysis. Mann-Whitney's *U* test (distribution-free) was used in **Figure 1b**, based on large sample sizes and non-normal distributions. This test was non-blinded; to avoid any biases in our analyses, we took images for all areas with labeled neurons and all labeled neurons were analyzed. The sample size was large enough (biological replicates, $n = 63–167$) to show statistical significance ($P < 0.001$). Criteria for data exclusion (for **Figs. 5** and **6**) are explained in the main text and figure legends. Exclusion of poor data in these experiments does not affect the conclusion. No data points were excluded in other data sets. Data are indicated as mean ± s.d. (for biological replicates) or mean ± s.e.m. (for technical replicates) only when normal distribution is applicable.

49. Lin, D.M. *et al.* Formation of precise connections in the olfactory bulb occurs in the absence of odorant-evoked neuronal activity. *Neuron* **26**, 69–80 (2000).
50. Saito, T. *In vivo* electroporation in the embryonic mouse central nervous system. *Nat. Protoc.* **1**, 1552–1558 (2006).

doi:10.1038/nn.3447